EXAMINING THE NATURE OF TWO-DIMENSIONAL TRANSVERSE WAVES IN MARGINAL HYDROGEN DETONATIONS USING BOUNDARY LAYER LOSS MODELING WITH DETAILED CHEMISTRY

Smith, J.G.[1,*], Schmitt, C.[1], Xiao, Q.[2], and Maxwell, B.M.[1,3]
[1]Department of Mechanical and Aerospace Engineering, Case Western Reserve University, 10900 Euclid Avenue, Glennan 418, Cleveland Ohio, 44106, USA
[2]National Key Laboratory of Transient Physics, Nanjing University of Science and Technology, Nanjing, China
[3]Department of Mechanical Engineering, University of Ottawa, 161 Louis Pasteur, Ottawa, K1N 6N5, Canada
[*] jgs121@case.edu

ABSTRACT

Historically, it has been a challenge to simulate the experimentally observed cellular structures and marginal behavior of multidimensional hydrogen-oxygen detonations in the presence of losses, even with detailed chemistry models. Very recently, a quasi-two-dimensional inviscid approach was pursued where losses due to viscous boundary layers were modeled by the inclusion of an equivalent mass divergence in the lateral direction using Fay's source term formulation with Mirels' compressible boundary layer solutions. The same approach was used for this study along with the inclusion of thermally perfect detailed chemistry in order to capture the correct ignition sensitivity of the gas to dynamic changes in the thermodynamic state behind the detonation front. In addition, the strength of transverse waves and their impact on the detonation front was investigated. Here, the detailed San Diego mechanism was applied and it has been found that the detonation cell sizes can be accurately predicted without the need to prescribe specific parameters for the combustion model. For marginal cases, where the detonation waves approach their failure limit, quasi-stable mode behavior was observed where the number of transverse waves monotonically decreased to a single strong wave over a long enough distance. The strong transverse waves were also found to be slightly weaker than the detonation front, indicating that they are not overdriven, in agreement with recent studies.

1. INTRODUCTION

This study seeks to use a novel numerical simulation methodology to better understand marginal detonation behavior in thin planar channels. In particular, the study aims to investigate the nature of strong transverse reaction waves at the critical near-failure limit, a regime that is characteristic of having large transient pressure spikes. Early experiments investigating marginal detonation were conducted using small round tubes and low quiescent pressures, which approached the quenching limit below which detonations fail to propagate. Such limiting detonation waves were found to exhibit unique behaviors that were described as both spinning and galloping [1–3]. The galloping behavior, which can occur in both round tubes and rectangular (planar) channels, can be described as a phenomenon where the forward incident wave speed becomes periodically overdriven, as high as 1.5 times the theoretical Chapman-Jouguet (CJ) velocity, but then degenerates to a velocity well below this theoretical value for most of the cycle [4]. This extreme velocity change is also typically accompanied by a monotonic degeneration of the number of transverse waves [5]. The fundamental difference between marginal detonations in round tubes and rectangular planar channels is that marginal detonations in tubes were found to include a continually *spinning* transverse detonation component [6], while marginal planar detonations were found to

intermittently exhibit transverse detonations only at the beginning of each cycle [7]. These transverse detonations were found to trigger ignition perpendicular to the mean flow [6–9], and are believed to be key features permitting sustenance of the detonation wave propagation in critical limiting conditions. While it is known that excess inert gas dilution can stabilize certain reactive mixtures and suppress galloping behavior [4], the exact conditions that permit intermittent strong reactive transverse waves are not well understood, and are difficult to predict. In addition, it is unknown whether such transverse waves are actually overdriven with respect to the the mixture through which they propagate, or not.

To date, most of the multi-dimensional simulations of hydrogen detonation waves in thin channels rely on solving the reactive Euler flow equations with the simple one-step global Arrhenius reaction kinetics. This is presumably due to the prohibitive computational cost of resolving the full three-dimensional flow field using the Navier-Stokes equations. However, extensive numerical simulation efforts [10, 11] have shown that the simulated detonation cells tend to be smaller than those measured experimentally from narrow channels. To clarify such inconsistency between numerics and experiments in terms of detonation cell sizes, one school of thought [11–13] points out the potentially significant role of detailed chemistry and the non-equilibrium effects. On the other hand, Xiao and Weng [14] have explicitly demonstrated the effect of losses on detonation cell sizes, particularly near the propagation limit, due to the significantly increased detonation velocity deficits resulting in the notably lengthened detonation reaction zones. Such detonation characteristic length scale dependence on losses has also been shown earlier by Radulescu et al. [15, 16] in their slowly diverging channel experiments, which follows the exponential relationship governed by the mixture's effective activation energy. Furthermore, to account for the presence of losses, Xiao et al. [17] proposed to model the effect of boundary layers on argon-diluted hydrogen-oxygen detonations propagating in thin channels, by including an equivalent mass divergence in the lateral direction, akin to Fay's methodology of modeling boundary layer losses [18]. In their model, the Mirels' compressible laminar boundary layer theory [19] was adopted for quantifying the boundary-layer-induced loss and such formulation has been shown to excellently reproduce the cellular dynamics observed experimentally across a range of initial mixture pressures. However, their simulations employed a simplified perfect gas two-step combustion modeling approach, and thus did not contain the non-equilibrium effects and ignition sensitivity to the shocked gas that is believed necessary to correctly model transverse detonations at near-critical detonation limits [20]. As a result, the two-step approach required specific tuning of model parameters for each set of initial conditions, and was not able to properly capture the thermodynamic state in the shocked gas or combusted products, nor capture transverse detonations at the most critical near-failure propagation limits.

Therefore, the current study aims to extend the quasi-two-dimensional approach of Xiao et al. [17] to include detailed chemistry, in order to accurately model both the effects of boundary layers and the reaction phenomena leading to transverse reactive waves and their resulting cellular structures. The approach is first validated for diluted mixtures of the previous investigation ($2H_2 + O_2 + 7Ar$), and then extended to marginal conditions of a less diluted mixture and lower pressure, $2H_2 + O_2 + 2Ar$ at 2.1 kPa.

2. NUMERICAL MODELING APPROACH

2.1. Governing Equations

In the approach adopted here, the two-dimensional thin-channel detonation flow fields are modeled using the inviscid Euler equations, which account for the conservation of mass, momentum, total energy, and ith chemical species. In order to account for the presence of boundary layers in the lateral direction, in the Euler framework, source terms in the form of $\frac{1}{A}\frac{DA}{Dt}$ were included to model the equivalent mass divergence that would result from the displacement of streamlines in the boundary layer, and their associated equivalent hypothetical rate of area increase. The governing equations [21] in the presence of this

area increase are thus given by

$$\frac{\partial \rho}{\partial t} + \nabla \cdot (\rho \boldsymbol{u}) = -\rho \frac{1}{A} \frac{DA}{Dt} \tag{1}$$

$$\frac{\partial (\rho \boldsymbol{u})}{\partial t} + \nabla \cdot (\rho \boldsymbol{u} \otimes \boldsymbol{u}) + \nabla p = -\rho \boldsymbol{u} \frac{1}{A} \frac{DA}{Dt} \tag{2}$$

$$\frac{\partial (\rho E)}{\partial t} + \nabla \cdot \Big((\rho E + p) \boldsymbol{u} \Big) = -(\rho E + p) \frac{1}{A} \frac{DA}{Dt} \tag{3}$$

$$\frac{\partial (\rho Y_i)}{\partial t} + \nabla \cdot (\rho \boldsymbol{u} Y_i) = -\rho Y_i \frac{1}{A} \frac{DA}{Dt} + \dot{\omega}_i. \tag{4}$$

Here, ρ, $\boldsymbol{u}$, A, p, Y_i, and $\dot{\omega}_i$, refer to the density, velocity vector, channel cross-sectional area, pressure, mass fraction of the ith species, and the reaction rate of the ith species, respectively. The total specific energy, E, is defined as

$$E = \sum (Y_i h_i) - \frac{p}{\rho} + \frac{1}{2} |\boldsymbol{u}|^2, \tag{5}$$

where h_i is the enthalpy of the ith species. The ideal gas law is used as the equation of state with its corresponding equation for the chemically frozen speed of sound, c, given below as

$$p = \rho R T, \tag{6}$$

$$c^2 = \gamma p / \rho, \tag{7}$$

where γ is the specific heat ratio. The specific heat capacities and enthalpies were calculated using the temperature-dependent, 7-coefficient NASA polynomial approximations [22]. As the channel height is larger than the width by more than an order of magnitude, boundary layer effects on the top and bottom of the channel could be considered negligible for this study.

Using a shock-attached reference frame with a quasi-steady-state assumption, and inserting an expression for the displacement thickness from Mirels' compressible laminar boundary layer solutions [19] to Fay's boundary layer theory [18], the source term can finally be reduced to

$$\frac{1}{A} \frac{DA}{Dt} \approx \frac{K_M}{w} \sqrt{\frac{\nu_s}{t - t_s}}, \tag{8}$$

where K_M is Mirels' constant, w is the physical channel width, ν_s is the post-shock kinematic viscosity, and $t - t_s$ is the elapsed time since a Lagrangian particle has passed through the shock front. The shock time is effectively recorded when the shock passes over the quiescent gas, the moment when $P > 2P_0$. In our conservative framework, we let

$$\frac{\partial (\rho t_s)}{\partial t} + \nabla \cdot (\rho \boldsymbol{u} t_s) = -\rho t_s \frac{1}{A} \frac{DA}{Dt}, \tag{9}$$

which is mathematically equivalent to permitting advection of the particle shock time through

$$\frac{\partial t_s}{\partial t} + \boldsymbol{u} \cdot \nabla t_s = 0. \tag{10}$$

2.2. Solution Methods

The source terms in the conservation Eqs. (1) to (4) and (9) require three inputs for each set of initial conditions as shown in Eq. (8). The geometric channel width w is fixed, and the post-shock kinematic viscosity is calculated for the CJ state using Cantera [23] and SDToolbox [24]. Note that this value is marginally different from the actual post-shock kinematic viscosity of a shock with a velocity deficit, but the latter value cannot be determined theoretically as the velocity deficit is not known a priori. The only remaining unknown is Mirels' constant, K_M. For this study, theoretical values were calculated using the same procedure as from Xiao et. al [16] using the CJ speeds given by the detailed San Diego mechanism. $K_M \approx 4$ for all pressures considered where the mixture was $2H_2 + O_2 + 7Ar$.

The detailed San Diego combustion mechanism [25] implemented includes 8 reacting species (H_2, O_2, H, O, OH, HO_2, H_2O_2, and H_2O), an inert species (Ar), and 23 reversible, elementary reactions when only considering hydrogen oxidation.

The governing equations, Eqs. (1) to (4), were solved using the second-order HLLC method [21] with the van Albada slope limiter [26]. The Sundials CVODE solver [27] was used to implicitly solve a constant-volume combustion reaction in each cell for time-marching, and a Zel'dovich–von Neumann–Döring (ZND) reaction for solution initialization. Adaptive mesh refinement [28] was used near shocks and in reaction zones by refining in regions with large density gradients and high concentrations of radicals to allow lower mesh resolution in the rest of the domain. The domain was meshed with the same grid spacing in the x and y directions with up to seven levels of adaptive mesh refinement down to a minimum specified resolution. Four different minimum grid resolutions of 390.6, 195.3, 97.7, and 48.8 μm (later abbreviated to 391, 195, 98, and 49 μm for brevity) were used for this study. Depending on the initial pressure, these resolutions correspond to resolving 5 to 148 grids per induction length acquired through ZND solutions corresponding to waves computed at their velocity deficit. As inviscid simulations are known to qualitatively vary with resolution due to differences in numerical diffusion [20, 29], a resolution study was done for each pressure with a minimum of at least 20 grids per induction length reached based on the recommendations of previous studies [30, 31].

2.3. Domain, and Initial and Boundary Conditions

The computational domain used for this study was in the reference frame of the detonation front to reduce computational expenses. The computational length was 1.5 m, but the total effective distance covered by the detonation wave depended on the number of time steps, and was up to 15 m for lower initial pressures where the detonation front needed longer to settle to a quasi-steady state. Early comparisons were made with the absolute reference frame to ensure both approaches gave the same result. For two-dimensional simulations, the domain height was 200 mm to match the experimental domain [17]. The right bound was given a constant inflow boundary condition approximately equal to the average experimental wave speed to allow the detonation front to stay within the domain, while the left boundary was given a zero gradient boundary condition and was sufficiently far from the detonation front to prevent influencing the detonation dynamics as shown in Figure 1. The top and bottom bounds were given symmetry boundary conditions, and boundary layer effects were included via source terms for a 19 mm channel width in the third dimension.

The quiescent fluid at $x > 0$ was given a constant temperature of $T_0 = 300$ K and an initial pressure P_0, with the exception of the first four induction lengths (Δ_i), which were prescribed random density perturbations up to ±25% to encourage detonation cell formation. The domain at $x \leq 0$ was initialized with two different ZND solutions. From 0 to -0.25 m, a ZND structure was initialized corresponding to the CJ velocity with an overdrive ranging from 1.2 to 1.7 in order to overcome the typical startup errors that may arise due to the sharp discontinuity in the initial solution at $x = 0$. From -0.25 to -0.5

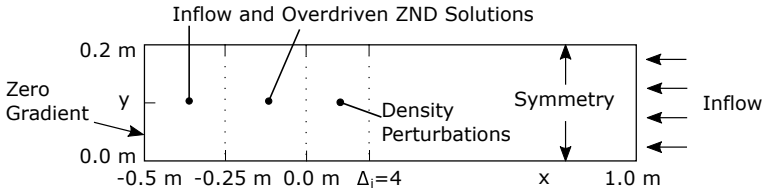

Figure 1: Computational domain in the detonation front wave reference frame.

m, a ZND structure corresponding to the inflow velocity was initialized. This discontinuity at -0.25 m allowed for an expansion wave to propagate towards the detonation front in order to allow it to settle to its quasi-steady speed more quickly.

Five initial pressures were investigated for this study with corresponding CJ velocities, experimental deficit velocities, induction lengths calculated from Cantera [23] and SDToolbox [24], and grids per induction length shown in Table 1. Data points were saved every 20 µs. All velocity deficit calculations were made by calculating the mean velocity of at least 100 data points along the bottom wall once the detonation wave had reached quasi-steady conditions to ensure enough detonation wave cycles were captured.

Table 1: Theoretical CJ velocity, experimental velocity with deficit [14, 17], induction length, and grids per induction length for each initial pressure and mixture at T_0 = 300 K. The induction lengths correspond to the ZND structure calculated for the deficit velocities rather than the CJ velocities.

					Grids per Induction Length			
P_0 (kPa)	Mixture	D_{CJ} (m/s)	D_{def} (m/s)	L_{ind} mm	391µm	195µm	98µm	49µm
2.1	$2H_2 + O_2 + 2Ar$	1891.3	1569.8	19.02	48.7	97.4	N/A	N/A
3.1	$2H_2 + O_2 + 7Ar$	1593.9	1211.4	33.52	85.8	N/A	N/A	N/A
4.1	$2H_2 + O_2 + 7Ar$	1601.9	1329.5	14.40	36.9	73.7	147.5	N/A
6.9	$2H_2 + O_2 + 7Ar$	1616.6	1422.6	4.72	12.1	24.2	48.4	96.7
10.3	$2H_2 + O_2 + 7Ar$	1628.0	1497.8	2.05	5.2	10.5	21.0	42.0

3. RESULTS AND DISCUSSION

3.1. Theoretical and Tuned K_M Values

The theoretical values for K_M were calculated for each reactive mixture using the frozen shock state of the mixture with variable heat capacities according to the procedure by Xiao and Radulescu [16]. These values were $K_M \approx 4$ for all of the pressures with the $2H_2 + O_2 + 7Ar$ mixture and $K_M = 4.32$ for $P_0 = 2.1$ kPa with the less diluted $2H_2 + O_2 + 2Ar$ mixture. Exact values are given below in Table 2. Using these values, a one-dimensional resolution study was completed comparing the velocity deficit for all four resolutions with a maximum error of 0.75% between 390.6 and 48.8 µm being recorded for the three highest initial pressures as seen below in Figure 2. Although the velocity deficits were essentially grid independent, they did not match the experimental velocity deficits from Xiao et al. [17]. In addition, detonations at $P_0 = 4.1$ kPa could only be averaged for a few cell cycles before they ultimately failed which limited the accuracy of the deficit calculation at that pressure. At 2.1 and 3.1 kPa, detonations could not be sustained at all.

To better match experiments, a parametric study was done in two-dimensional simulations to tune the values of K_M to yield the correct velocity deficits as was done previously for the two-step modeling approach in the study by Xiao et al. [17]. Figure 2 shows the results of these values being tuned to within 1% of experiments at 97.7 µm with the final tuned K_M values being seen in Table 2 alongside the

tuned values of the prior two-step approach. Note that K_M for $P_0 = 2.1$ kPa had not converged through 195.3 µm and the proper velocity deficit for $P_0 = 3.1$ kPa at 195.3 µm could not be reached without the detonation failing.

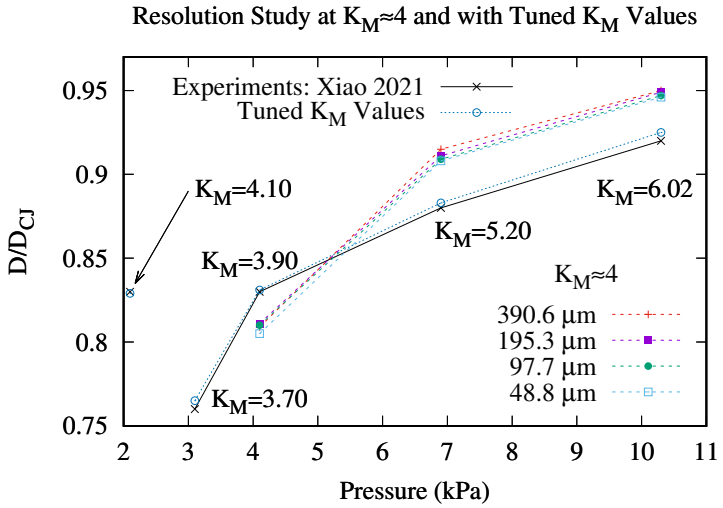

Figure 2: Resolution study of the velocity deficit for $K_M \approx 4$ compared to experiments [14, 17]. Note that detonations at $P_0 = 3.1$ and 2.1 kPa failed completely, and at 4.1 kPa failed after a few cell cycles. Also includes velocity deficits for tuned values of K_M.

Table 2: Theoretical and tuned Mirels' constants for two-step [17] and detailed chemistry. $*$ Only at 195.3 µm. † Only at 390.6 µm

	K_M Values		
P_0 (kPa)	Theoretical	Tuned: Two-Step Chemistry	Tuned: Detailed Chemistry
2.1	4.32	N/A	4.10*
3.1	3.98	N/A	3.70†
4.1	3.99	1.75	3.90
6.9	4.01	2.50	5.20
10.3	4.03	2.50	6.02

It can be seen that the tuned K_M values tend to increase for increasing initial pressures for a given mixture and have values for detailed chemistry much higher than for the two-step chemistry approach, a discrepancy which can only be attributed to the different reaction kinetics and thermodynamic properties applied. The values match reasonably well for detailed chemistry at $P_0 = 2.1$, 3.1, and 4.1 kPa. The cause of the larger error between the K_M values at 6.9 and 10.3 kPa is unknown, but could be due to ignoring conduction at the walls or to neglecting 3D effects which are more significant when the detonation cell sizes approach the channel thickness. These 3D effects would be more evidently pronounced for 6.9 and 10.3 kPa as the ratio of cell size to the channel width is less than 10 [32] allowing transverse waves to propagate in the third dimension. Xiao et al. also surmised that the assumptions of a quasi-steady shock and the use of analytical solutions to the boundary layers could be to blame for the errors in K_M [17].

3.2. Grid Resolution Effects on the Two-Dimensional Flow Fields

As seen in Table 3, the numerical velocity deficit is essentially resolution independent and matches experimental values well when using tuned K_M values for $P_0 = 4.1$ through 10.3 kPa, for the moderately

diluted mixture ($2H_2 + O_2 + 7Ar$). As noted previously, the K_M values for the $P_0 = 2.1$ and 3.1 kPa cases display a lack of resolution independence where the deficit velocity decreases or the detonation even fails at finer resolutions. This is possibly due to the greater dependence of the detonation front on the transverse waves for those pressures. This study also sought to see if the corresponding experimental detonation cell sizes could be predicted. Numerical schlieren images were extracted from the simulations from the density gradient and were compared to experimental schlieren images from two studies led by Xiao [14, 17] as seen in Figure 3. Cell size can be seen in Table 3 and was estimated from the finest resolution cases available for each initial pressure by the formula $\lambda = \frac{H}{0.5*N}$ where H is the channel height and N is the number of triple points counted in the channel.

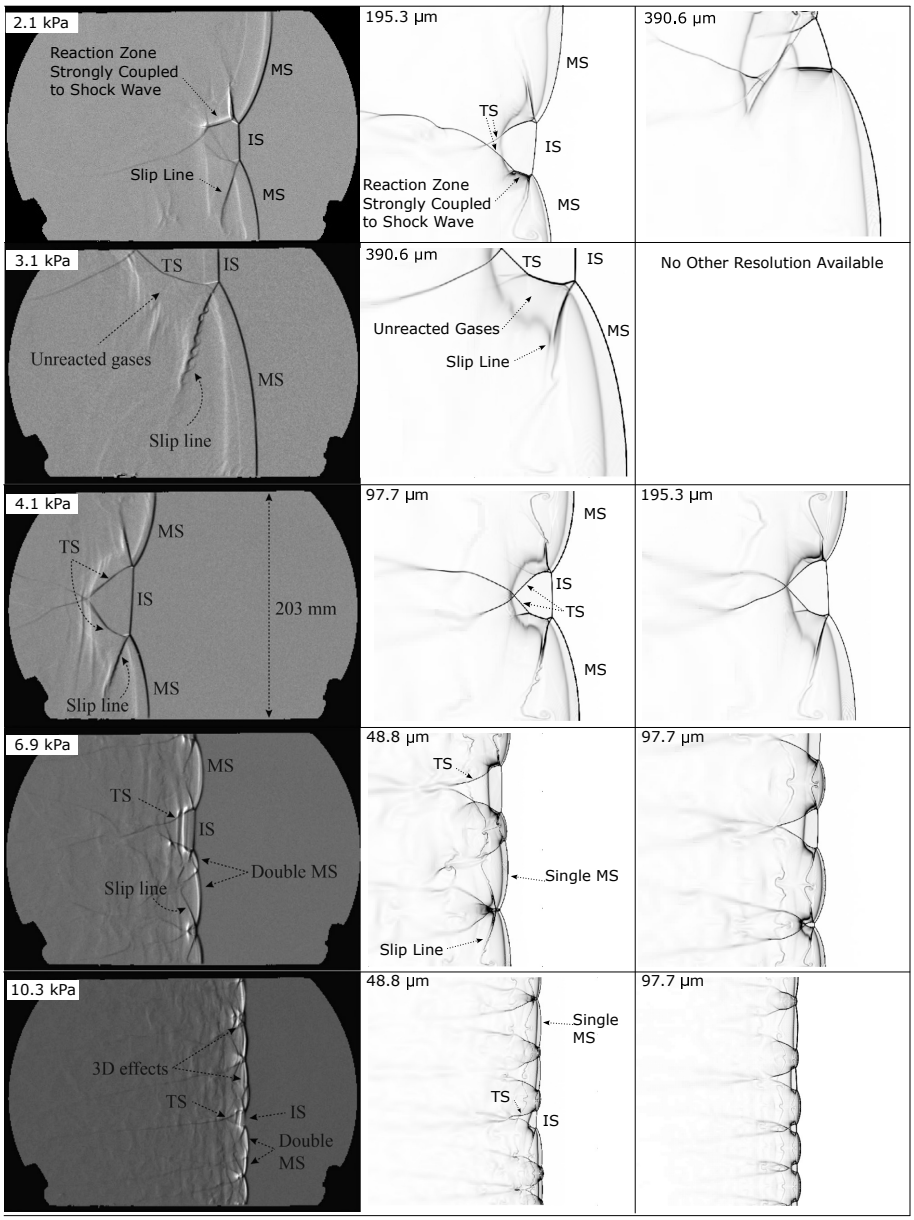

Figure 3: Experimental *(left column)* [14, 17] vs numerical schlieren for finest resolution *(middle column)* and next finest resolution *(right column)* for the five initial pressures with tuned K_M values.

Overall, it was found that when the experimental velocity deficit was matched using the tuned K_M values, the cellular structures could also be accurately predicted with resolutions fine enough to achieve grid independence as seen in the right two columns of Figure 3. As expected, the higher pressures

Table 3: Velocity deficits and cell sizes (mm) for each resolution (μm) for experiments [14, 17] vs two-dimensional simulations using the tuned K_M values. * For K_M = 4.20

P_0	D/D_{CJ}					Cell Size λ (mm)				
(kPa)	Exp.	391μm	195μm	98μm	49μm	Exp.	391μm	195μm	98μm	49μm
2.1	0.83	0.829*	0.826	N/A	N/A	~203	203~406	203~406	N/A	N/A
3.1	0.76	0.765	N/A	N/A	N/A	~406	~406	N/A	N/A	N/A
4.1	0.83	0.829	0.832	0.831	N/A	~203	203~406	203~406	203~406	N/A
6.9	0.88	0.890	0.886	0.883	0.884	68~81	41~51	68~102	68~102	68~102
10.3	0.92	0.927	0.923	0.925	0.923	31~41	0	23~25	37~41	37~41

needed finer resolutions to accurately resolve the hydrodynamic structures and settle to the correct cell size due to the shorter induction lengths. It should be noted that most simulations in Table 3 have a range of cell sizes. This is due to both the long distance needed for transverse waves to decay to quasi-steady-state, and in certain cases the existence of more than one quasi-stable mode where a certain number of transverse waves would exist for a few cycles before degenerating into a lower number of transverse waves. Such behavior was not widely observed in the experiments as schlieren images were only taken at a single location within the 3.4 m channel and so any quasi-stable modes existing before or after the observation window were missed. In contrast, the simulations permitted a propagation distance of up to 15 m, which allowed the progression through multiple modes, and enabled investigation of the change in transverse wave dynamics as the modes degenerated towards a single transverse wave.

3.3. The Marginal Detonation Behavior

Having captured the correct experimental velocity deficit and cellular structure behavior, attention was turned towards potential marginal behavior for the P_0 = 2.1, 3.1, and 4.1 kPa cases, which were all close to the detonation failure limits. For 2.1 and 4.1 kPa, instabilities and asymmetries led to the occasional formation of strong transverse waves that were strongly coupled to the reaction zone. The 3.1 kPa case, though seemingly closer to the detonation limit than the 4.1 kPa case, did not display similar behavior. In Figure 4 below for 2.1 kPa at 390.6 μm it can be seen that a seemingly stable mode of two transverse waves can spontaneously transform into a single transverse wave mode with strong coupling between the shock wave and the reaction zone. The top transverse wave in frame *a)* can be seen gradually decaying in frames *b)* through *d)* before it completely disappears by frame *e)* once the stronger transverse wave has overtaken it. This behavior is similar to the description of quasi-steady galloping waves given by Vasil'ev [5], with the key difference being that no complete quenching and re-initiation characteristic of true galloping was observed in this study. This assessment agrees with experimental evidence which indicates that highly argon-diluted hydrogen mixtures do not exhibit a true galloping behavior [4].

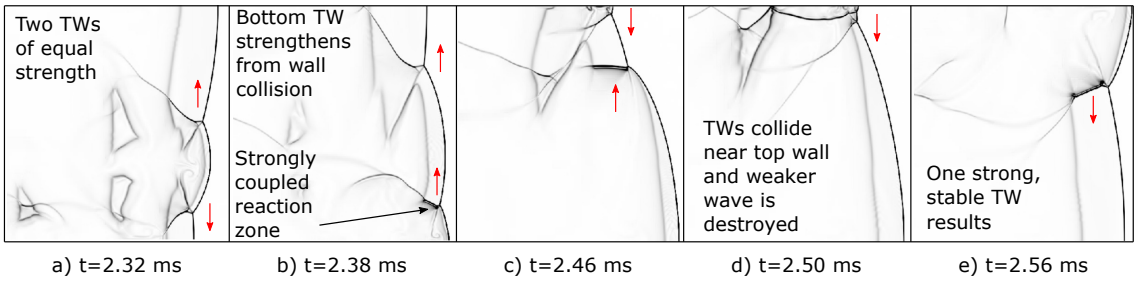

Figure 4: Numerical schlieren at 2.1 kPa with K_M=4.20 at 390.6 μm for gradual transition from *a)* two transverse waves to *e)* one strong transverse wave. Direction of transverse waves noted with red arrows.

The spontaneous creation of a strong transverse wave also seems to be somewhat dependent on reso-

lution. For 4.1 kPa, the transition from two waves to one occurred at 15.2, 10.4, and 9.6 m down the channel respectively for 390.6, 195.3, and 97.7 μm resolutions, although the second wave reappeared after one cycle for the 390.6 μm case. We note here, that no such transition was observed in the experiments, which were only visualized within a 3.4 m long channel. The decrease in numerical diffusion or the increased number of initial density perturbations could both be potential causes of the faster transitions from two transverse waves to one seen at finer resolutions. Physically, it is possible that both the boundary layer losses and asymmetry between the two transverse wave speeds allowed for the stronger wave to overtake the weaker wave, and played a role in this eventual mode degeneration.

The evidence of these strong transverse waves can also be seen in Figure 5a where the velocity of the detonation front can be seen varying from 151% to 71% of the average velocity for P_0 = 2.1 kPa in comparison to only 117% to 90% for 10.3 kPa. This trend is also visible for non-dimensional over-pressure in Figure 5b where 2.1 kPa exhibits over-pressures up to $\frac{P-P_0}{P_0}$ =146 in the later part of the plot where the single wave mode has formed, in comparison to maximum over-pressures of up to 96 for the P_0 = 10.3 kPa case.

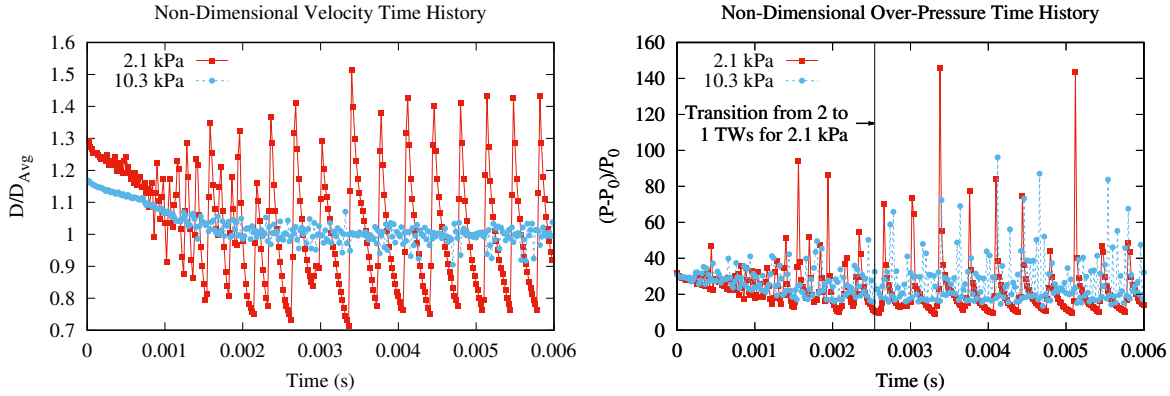

(a) Non-dimensional velocity.

(b) Non-dimensional over-pressure.

Figure 5: Time histories along the channel bottom wall for $2H_2 + O_2 + 2Ar$ at 2.1 kPa, 195.3 μm and $2H_2 + O_2 + 7Ar$ at 10.3 kPa, 48.8 μm.

Figure 6 compares the differences in initial pressures and mixtures by showing the averages of all the over-pressure maximums for the over-pressure time histories. In general, the average and the standard deviation of over-pressure maximums display an increasing trend as the initial pressure decreases, but the P_0 = 3.1 kPa case clearly seems to be an outlier. The cause of this discrepancy is unknown, but may be due to the fact that the 3.1 kPa case never displays the quasi-stable two wave to one wave mode degeneration suggesting that some sort of coupling between the two waves may occur during the formation of one strong wave. Since the value of K_M at 3.1 kPa could not be successfully converged with increasing resolution due to failing detonations, it is also possible that too much numerical diffusion is artificially stabilizing the detonation and preventing true marginal behavior from occurring. In addition to pressure trends, the clearest marginal behavior was found to exist for the less diluted case at P_0 = 2.1 kPa ($2H_2 + O_2 + 2Ar$) which had the largest over-pressure maximum and standard deviation.

Measurements were also made to compare the strength of transverse waves to that of the detonation front for the three lowest initial pressures. The triple point attached to the transverse wave was chosen as the measurement location as it is well-defined in space and is representative of the transverse wave speed. The velocity vector of the triple point was first calculated from position data across time steps using a 1st order central difference approximation. A rectangular portion of the unburned, shocked gas directly in front of the wave was then sampled to find the mass-weighted-averaged velocity vector and temperature, and the ensemble-averaged pressure for that region as per the procedure given by Floring

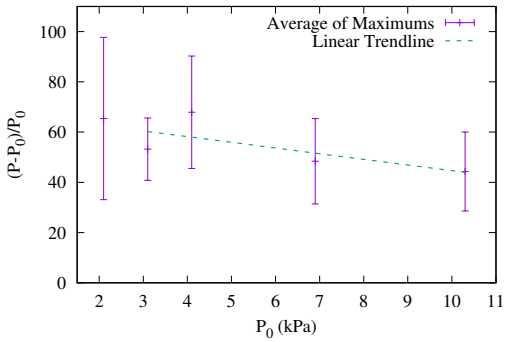

Figure 6: Non-dimensional over-pressure maximum averages with the error bar indicating the standard deviation. Trend line is for cases corresponding to the $2H_2 + O_2 + 7Ar$ mixture

et al. [20]. Each rectangle contained a range of 6,600 to 64,000 grid points depending on the size of the transverse wave and the resolution of each specific case. The CJ velocity was found using these values of the averaged pressure and temperature, and the unburned composition. The velocity vector of the unburned gas was then subtracted from the velocity vector of the triple point as seen in Figure 7a to find the velocity of the triple point relative to the unburned gas. Finally, this relative velocity was divided by the CJ velocity of the unburned gas to find the strength of the transverse wave.

The resulting transverse wave strengths for $P_0 = 2.1$, 3.1, and 4.1 kPa can be seen in Figure 7b through Figure 7d. Several wave cycles are included for each quasi-stable mode with two and one wave modes being captured for 2.1 and 4.1 kPa. In general, it was found that the transverse waves travel at or below the deficit velocity of the detonation front. Therefore, the transverse waves are found not to be overdriven. However, the transverse wave in the one wave mode was found to be somewhat stronger than in the two wave mode. For the 2.1 kPa case, the mean value of $\frac{D}{D_{CJ}}$ for the transverse waves for the one and two wave modes were 0.75 and 0.69, respectively, in comparison to the detonation front which showed a value of 0.86. The 3.1 and 4.1 kPa cases displayed similar trends. Notably, for all three initial pressures, the transverse wave mean strengths were all approximately 12% lower than the detonation front strengths for the one transverse wave mode, and all approximately 19% lower for the two transverse wave mode.

Two recent numerical studies, which included no losses, investigated the role of transverse waves in critical hydrocarbon detonation re-initiation due to diffraction [33] and interaction with an obstacle [20]. Both studies performed the same transverse wave strength calculation as done above and concluded that the transverse waves traveled at the CJ velocity with respect to the shocked, unburned gases following the detonation front. This conclusion indicated that the transverse waves traveled with less strength than the overdriven detonation fronts. This is consistent with the findings in the current study.

4. CONCLUSIONS

This study determined that for detailed chemistry, Fay's source term formulation is able to accurately predict the cellular structure provided that Mirels' constant K_M is slightly tuned to match the experimental velocity deficit. In general, K_M seemed to require less tuning for detailed chemistry than for simplified two-step chemistry. For $P_0 = 2.1$ kPa, the tuned value of K_M was found to decrease with resolution while the detonation for the 3.1 kPa case could not be sustained at resolutions finer than 390.6 μm. Both effects are possibly due to decreasing numerical diffusion with finer resolutions.

For marginal detonations, two-dimensional simulations were found to sustain detonations at higher K_M values than one-dimensional simulations indicating that transverse waves play a major role in stabilizing the detonation front. In addition, strong transverse waves tightly coupled to the reaction zone with large

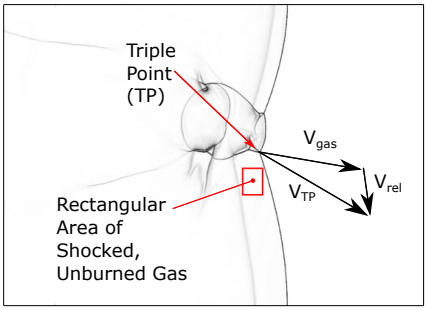

(a) Triple point relative velocity vector diagram.

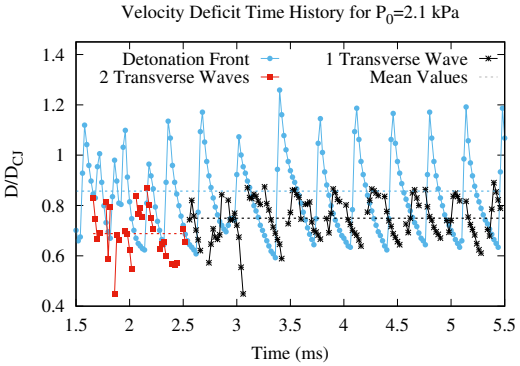

(b) P_0 = 2.1 kPa at 195.3 µm for K_M =4.10.

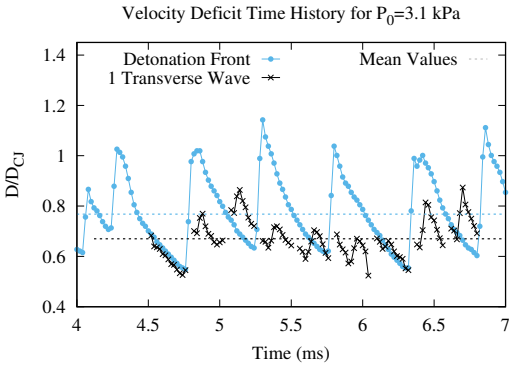

(c) P_0 = 3.1 kPa at 390.6 µm for K_M =3.70.

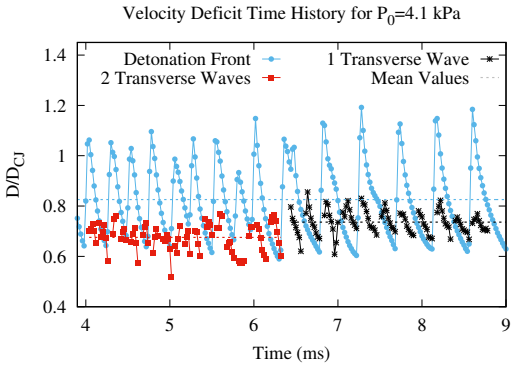

(d) P_0 = 4.1 kPa at 97.7 µm for K_M =3.90.

Figure 7: Detonation front and transverse wave velocity calculations.

over-pressures were sometimes able to form when the number of transverse waves degenerated from two to one. The average and standard deviation of the maximum over-pressures were in general found to increase as the initial pressure and the argon dilution decreased. The P_0 = 3.1 kPa case was an exception to this trend possibly indicating that more than one wave mode is required to produce large over-pressures. However, the detonations for this case also failed at finer resolutions possibly due to reduced numerical diffusion. Further investigations are likely required, and may need to explicitly model diffusion and examine more transverse wave cycles.

Lastly, the strength of these strong transverse waves was found to be slightly less than the detonation front, even for the single wave mode, indicating that the transverse waves are not overdriven. This result matches the findings of recent studies investigating detonation re-initiation. In addition, the transverse wave strength was found to be higher for the one wave mode than for the two wave mode.

ACKNOWLEDGEMENTS

J.G. Smith would like to thank M. Peswani and B. Schmidt for their guidance and support. J.G. Smith also acknowledges support from the Office of Naval Research grant no. N00014-23-1-2048 for this work. This work made use of the High Performance Computing Resource in the Core Facility for Advanced Research Computing at Case Western Reserve University.

REFERENCES

1. Mooradian, A. and Gordon, W., Gaseous detonation. I. Initiation of detonation. *The Journal of Chemical Physics*, 1951, **19, no. 9**, pp. 1166–1172.
2. Duff, R., Knight, H. and Wright, H., Some detonation properties of acetylene gas. *The Journal of Chemical Physics*, 1954, **22, no. 9**, pp. 1618–1619.

3. Manson, N., Brochet, C., Brossard, J. and Pujol, Y., Vibratory phenomena and instability of self-sustained detonations in gases. *Symposium (International) on Combustion*, 1963, **9, no. 1**, pp. 461 – 469.
4. Gao, Y., Ng, H. and Lee, J., Experimental characterization of galloping detonations in unstable mixtures. *Combustion and Flame*, 2015, **162, no. 6**, pp. 2405 – 2413.
5. Vasil'ev, A., Quasi-steady regimes of wave propagation in active mixtures. *Shock Waves*, 2008, **18, no. 4**, pp. 245–253.
6. Voitsekhovskii, B., Mitrofanov, V. and Topchian, M., Investigation of the structure of detonation waves in gases. *Symposium (International) on Combustion*, 1969, **12, no. 1**, pp. 829 – 837.
7. Strehlow, R. and Crooker, A., The structure of marginal detonation waves. *Acta Astronautica*, 1974, **1, no. 3**, pp. 303–315.
8. Subbotin, V., Two kinds of transverse wave structures in multifront detonation. *Combustion, Explosion and Shock Waves*, 1975, **11**, pp. 83–88.
9. Gamezo, V.N., Vasil'ev, A.A., Khokhlov, A.M. and Oran, E.S., Fine cellular structures produced by marginal detonations. *Proceedings of the Combustion Institute*, 2000, **28, no. 1**, pp. 611–617.
10. Oran, E., Weber, J., Stefaniw, E., Lefebvre, M. and Anderson, J., A numerical study of a two-dimensional H2-O2-Ar detonation using a detailed chemical reaction model. *Combustion and Flame*, 1998, **113, no. 1**, pp. 147–163.
11. Taylor, B., Kessler, D., Gamezo, V. and Oran, E., Numerical simulations of hydrogen detonations with detailed chemical kinetics. *Proceedings of the Combustion Institute*, 2013, **34, no. 2**, pp. 2009 – 2016.
12. Voelkel, S., Masselot, D., Varghese, P. and Raman, V., Analysis of hydrogen-air detonation waves with vibrational nonequilibrium. *AIP Conference Proceedings*, 2016, **1786, no. 1**, p. 070015.
13. Shi, L., Shen, H., Zhang, P., Zhang, D. and Wen, C., Assessment of vibrational non-equilibrium effect on detonation cell size. *Combustion Science and Technology*, 2017, **189, no. 5**, pp. 841–853.
14. Xiao, Q. and Weng, C., Effect of losses on hydrogen–oxygen–argon detonation cell sizes. *Physics of Fluids*, 2021, **33, no. 11**, p. 116103.
15. Radulescu, M. and Borzou, B., Dynamics of detonations with a constant mean flow divergence. *Journal of Fluid Mechanics*, 2018, **845**, p. 346–377.
16. Xiao, Q. and Radulescu, M., Dynamics of hydrogen–oxygen–argon cellular detonations with a constant mean lateral strain rate. *Combustion and Flame*, 2020, **215**, pp. 437–457.
17. Xiao, Q., Sow, A., Maxwell, B. and Radulescu, M., Effect of boundary layer losses on 2D detonation cellular structures. *Proceedings of the Combustion Institute*, 2021, **38, no. 3**, pp. 3641–3649.
18. Fay, J., Two-dimensional gaseous detonations: Velocity deficit. *The Physics of Fluids*, 1959, **2, no. 3**, pp. 283–289.
19. Mirels, H., Boundary layer behind shock or thin expansion wave moving into stationary fluid. Tech. Rep. TN-3712, NASA, 1956.
20. Floring, G., Peswani, M. and Maxwell, B., On the role of transverse detonation waves in the re-establishment of attenuated detonations in methane–oxygen. *Combustion and Flame*, 2023, **247**, p. 112497.
21. Toro, E., Riemann Solvers and Numerical Methods for Fluid Dynamics: A Practical Introduction. Springer, 3rd ed., 2009.
22. Kee, R., Rupley, F., Meeks, E. and M., J., CHEMKIN-III: A FORTRAN chemical kinetics package for the analysis of gas-phase chemical and plasma kinetics. Tech. rep., Sandia National Labs., Livermore, CA (United States), 1996.
23. Goodwin, D., Speth, R., Moffat, H. and Weber, B., Cantera: An object-oriented software toolkit for chemical kinetics, thermodynamics, and transport processes, 2018.
24. Shepherd, J., Shock & detonation toolbox—cantera 2.1. *Explosion Dynamics Laboratory, California Institute of Technology, accessed Oct*, 2018, **11**, p. 2019.
25. University of California at San Diego, Chemical-kinetic mechanisms for combustion applications. San Diego Mechanism web page, Mechanical and Aerospace Engineering (Combustion Research), University of California at San Diego, 2016.
26. van Albada, G., van Leer, B. and Roberts Jr., W., A comparative study of computational methods in cosmic gas dynamics. *Astron. Astrophys.*, 1982, **108**, pp. 76–84.
27. Hindmarsh, A., Brown, P., Grant, K., Lee, S., Serban, R., Shumaker, D. and Woodward, C., SUNDIALS: Suite of nonlinear and differential/algebraic equation solvers. *ACM T. Math. Software*, 2005, **31**, pp. 363–396.
28. Falle, S. and Giddings, J., Body capturing using adaptive cartesian grids. In M.J. Baines and K.W. Morton, eds., Numerical Methods for Fluid Dynamics IV, Oxford University Press, pp. 337–343, 1993.
29. Radulescu, M. and Maxwell, B., The mechanism of detonation attenuation by a porous medium and its subsequent reinitiation. *Journal of Fluid Mechanics*, 2011, **667**, p. 96–134.
30. Hwang, P., Fedkiw, R., Merriman, B., Aslam, T., Karagozian, A. and Osher, S., Numerical resolution of pulsating detonation waves. *Combustion Theory and Modelling*, 2000, **4, no. 3**, pp. 217–240.
31. Sharpe, G., Transverse waves in numerical simulations of cellular detonations. *Journal of Fluid Mechanics*, 2001, **447**, p. 31–51.
32. Voytsekhovskiy, B., Mitrofanov, V. and Topchiyan, M., Struktura fronta detonatsii v gazakh [The structure of a detonation front in gases]. In Doklady Akademii Nauk SSSR [Proceedings of the USSR Academy of Sciences], 1963 pp. 1–168.
33. Peswani, M. and Maxwell, B., Detonation wave diffraction in stoichiometric c2h4/o2 mixtures using a global four-step combustion model. *Physics of Fluids*, 2022, **34, no. 10**, p. 106104.